Vascular Structure Design of an Artificial Tree for Microbial Cell Cultivation and Biofuel Production

Thomas E. Murphy, Evan Fleming & Halil Berberoglu

Transport in Porous Media

ISSN 0169-3913

Transp Porous Med
DOI 10.1007/s11242-014-0318-3

Springer

Transp Porous Med
DOI 10.1007/s11242-014-0318-3

Vascular Structure Design of an Artificial Tree for Microbial Cell Cultivation and Biofuel Production

Thomas E. Murphy · Evan Fleming · Halil Berberoglu

Received: 3 September 2013 / Accepted: 21 April 2014

Abstract This paper reports the design of a vascular structure for an artificial tree, also known as an evaporation-driven porous substrate bioreactor (PSBR), for efficient biofuel production using microalgae. This system consists of multiple vertical ribs, each of which is made of porous membrane and grows algal cells on its surface as a biofilm. Nutrient medium flow through the reactor is driven by evaporation at the terminal end of the porous membrane, and nutrients are delivered from the porous membrane to the cells by diffusion. Flow through the membrane was modeled as a function of the physico-chemical and morphological properties of the membrane, as well as the environmental parameters governing evaporation. It was determined that under typical operating conditions, the evaporative flux from the evaporator region ranged from about 14 to 66 mg/m^2 s. Moreover, there was a membrane pore radius that maximized nutrient medium flow as a result of the competition between capillary, viscous, and gravitational forces. For the range of evaporative fluxes observed in this study, this pore radius was about 10 μm. Furthermore, a design example is provided for artificial trees made of three different commercially available membrane materials. A design methodology was demonstrated for maximizing photosynthetic productivity by tuning the evaporation-driven flow rate to ensure sufficient nutrient delivery to cells without incurring large evaporative loss rates. It was observed that both the growth rate and the evaporation-driven nutrient delivery rate were directly related to the irradiance in outdoor artificial trees, which provides a passive and efficient nutrient delivery mechanism. It is expected that the design principles along with the physical models governing the fluid flow in these vascular structures will aid researchers in developing novel applications for artificial trees.

Keywords Algae cultivation · Artificial tree · Evaporation · Attached cultivation · Capillary physics

T. E. Murphy · E. Fleming · H. Berberoglu (✉)
Mechanical Engineering Department, The University of Texas at Austin,
204 E. Dean Keeton St., Austin, TX 78712, USA
e-mail: berberoglu@mail.utexas.edu

Published online: 09 May 2014

Nomenclature

C	Constant of proportionality for calculating nutrient delivery length
$D_{\mathrm{w,a}}$	Diffusivity of water vapor in air (m^2/s)
G	Irradiance ($\mathrm{W/m}^2$)
Gr	Grashof number
h	Height (m)
h_{c}	Convection heat transfer coefficient ($\mathrm{W/m}^2$ K)
h_{fg}	Heat of vaporization (J/kg)
k	Hydraulic permeability (m^2)
k_{ω}	Mass transfer coefficient ($\mathrm{kg/m}^2$ s)
$\dot{m}'$	Mass flow rate per unit length (kg/s m)
$\dot{m}_{\mathrm{e}}''$	Evaporative flux ($\mathrm{kg/m}^2$ s)
P	Pressure (Pa)
P_{c}	Capillary pressure (Pa)
r	Pore radius
Re	Reynolds number
RH	Relative humidity
Sc	Schmidt number
Sh	Sherwood number
T	Temperature (K)
t	Rib thickness (m)
v_{w}	Wind speed (m/s)
$\dot{X}_o''$	Areal biomass production rate ($\mathrm{kg/m}^2$ s)
x	Distance in the direction of flow (m)
x_{c}	Critical wetting length (m)
x_{ND}	Nutrient delivery length (m)
$Y_{X/i_{\mathrm{L}}}$	Biomass yield based on nutrient i (kg/kmol)

Greek Symbols

α	Absorptivity
ϵ	Void fraction of porous membrane
μ	Dynamic viscosity (Pa s)
ω	Mass fraction
ρ	Mass density ($\mathrm{kg/m}^3$)
σ	Surface tension (N/m)
θ	Contact angle (°)

Subscripts

∞	Refers to ambient
a	Refers to air
e	Refers to exterior region
f	Refers to forced convection
i	Refers to interior region
L	Refers to limiting nutrient
n	Refers to natural convection
r	Refers to rib

1 Introduction

Algae cultivation is of commercial interest as its high photosynthetic productivity makes possible solar generation of biofuels (Chisti 2007; Clarens et al. 2010; Chisti and Yan 2011; Scott et al. 2010), as well as food, cosmetic, and pharmaceutical products (Pulz and Gross 2004; Spolaore et al. 2006; Milledge 2010; Day et al. 1999). Moreover, algae can utilize the nitrogen and phosphorous content of wastewater, enabling bioproduct formation using an otherwise untapped resource (Craggs et al. 2011; Kumar et al. 2011). Conventionally, algae have been grown in open ponds or closed photobioreactors, both of which require large volumes of water and large energy inputs for operation (Borowitzka 1999; Jorquera et al. 2010). In fact, the power required to operate most cultivation platforms exceeds the power embedded in the resultant biomass, precluding their use in sustainable biofuel generation (Clarens et al. 2010; Beal et al. 2011).

More recently, Porous Substrate Bioreactors (PSBRs) have been demonstrated as energy and water efficient systems that cultivate algae as biofilms on porous membranes (Murphy et al. 2012; Naumann et al. 2013; Liu et al. 2013). PSBRs increase the ratio of biomass to water in the system by a factor of about 30 compared to planktonic photobioreactors (Murphy et al. 2012), which reduces both the energy required for pumping and mixing the culture, as well as the energy required for downstream dewatering and biomass harvesting (Beal et al. 2011; Ozkan et al. 2012). Moreover, in a subclass of PSBRs, termed evaporation-driven PSBRs, flow through the reactor is driven by evaporation from a terminal membrane region, eliminating the need for a pump altogether (Murphy et al. 2012). These passive systems are also referred to as artificial trees as the nutrient delivery mechanism mimics the natural process of transpiration.

For efficient operation of artificial trees, the rate of nutrient delivery to the cells should be equal to the nutrient consumption rate by the cells. In turn, the nutrient uptake by the cells is primarily a function of local photon availability (Murphy and Berberoglu 2014). In the artificial tree system considered in this study, delivery of dissolved nutrients to cells is accomplished by diffusion from the porous membrane to the biofilm. Thus, nutrient concentrations in the liquid flowing through the porous membrane decrease in the direction of flow. The characteristic length over which nutrients become exhausted in the direction of flow is, therefore, a function of the bulk flow rate through the porous membrane, which is controlled by the evaporation rate from the terminal end.

This paper focuses on the flow rate of nutrient medium through artificial trees as a function of the physico-chemical properties of the membrane, as well as the environmental parameters that govern evaporation from the terminal end. Moreover, this analysis is coupled with growth kinetics and nutrient diffusion models for avoiding nutrient delivery limitation to cells by matching the physical height of the artificial tree to the characteristic length of nutrient exhaustion in the flow direction. In this way, this analysis provides guidelines for designing optimized artificial trees in which nutrients are delivered to cells at optimal rates based on photon availability.

2 Analysis

Figure 1 shows a single rib of an artificial tree. A scaled up artificial tree consists of multiple parallel vertical ribs (Murphy et al. 2012). The exterior rib section has a height h_e, but the liquid only wets a critical wetting length of x_c as a result of the balance between capillary, viscous, and gravitational forces. Since the critical wetting length x_c changes as a function

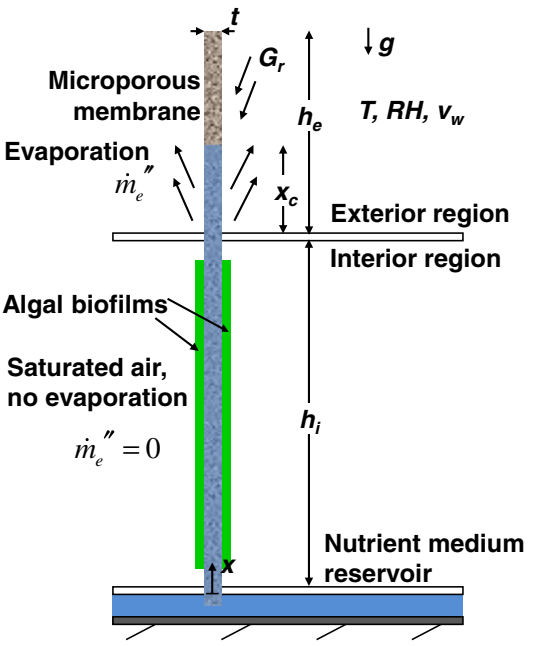

Fig. 1 Schematic of a single rib of an artificial tree

of environmental conditions, the exterior length h_e is designed to be equal to the maximum expected critical wetting length. The flow rate through the interior rib section, which has height h_i and hosts microbial growth, is then equal to the evaporation rate from the exterior rib section. The rib has a thickness t, an average pore radius r, and void fraction ϵ. The contact angle between the solid material of the rib and the liquid nutrient medium is θ. The gas surrounding the exterior section has temperature T, relative humidity RH, and velocity v_w in the direction into the page. The rib is illuminated with an irradiance G_r.

2.1 Assumptions

It is assumed that (1) the critical wetting length x_c and the evaporative flux $\dot{m}_e$ are at steady state as the time scale of environmental changes are large compared to the time scale of fluid motion, (2) the irradiance onto the rib is uniform, (3) the gas surrounding the interior rib section is saturated with water vapor at the biofilm surface temperature T_s, achievable through an environmental humidification system, resulting in zero evaporation from the interior surface, (4) the gas in both the interior and exterior regions is at atmospheric pressure, (5) the viscosity, density, surface tension, and contact angle with the porous material for the liquid medium flowing through the rib are equal to the respective properties for pure water, and (6) the pore size is uniform in the rib and equal to the average pore size of the membrane. A consequence of assumption (6) is that the porous membrane below the critical wetting length is completely saturated with liquid, whereas above the wetting length, the membrane is completely void of water. In real membranes, there will be a pore size distribution about the mean pore size, and as a result, a partially saturated condition will occur around the critical wetting length. Due to small deviation of pore sizes around the mean, these effects of relative permeability and partial saturation on flow rate are expected to be negligible.

2.2 Governing Equations

The flow rate of nutrient medium through the porous membrane is governed by the capillary pressure at the interface between the liquid and air at the critical wetting length (pulling upward), the viscous pressure drop along the flow path (pulling downward), and the gravitational force (pulling downward). Moreover, in the exterior region, the flow rate decreases in the direction of flow as a result of evaporation. The flow rate decreases to zero at the critical wetting length. Thus, the flow rate through the rib and the critical wetting length are interdependent. The upward mass flow rate per unit depth into the page, $\dot{m}'(x)$, can be written as,

$$\dot{m}'(x) = 2\dot{m}_e''x_c \text{ for } 0 \le x \le h_i \tag{1}$$

$$\dot{m}'(x) = 2\dot{m}_e''(x_c - (x - h_i)) \text{ for } h_i \le x \le h_i + x_c \tag{2}$$

where $\dot{m}_e''$ is the evaporative flux from the exterior rib. Equation (1) states that the flow rate through the interior region is equal to the evaporation rate from the exterior section. The factor of two results from the fact that water evaporates from both sides of the rib. Moreover, Equation (2) states that in the exterior rib region, the flow rate decreases linearly, from the interior flow rate at the interface between the interior and exterior sections, to zero at the critical wetting length.

Calculation of the flow rate requires first calculating the critical wetting length x_c. This is accomplished by equating the capillary pressure to the sum of the gravitational and viscous pressure drops along the flow path. First, the pressure gradient along the liquid flow path is given by the Darcy equation (Kaviany 1999),

$$\frac{dP}{dx} = -\frac{\mu}{tk\rho}\dot{m}'(x) - \rho g \tag{3}$$

where dP/dx is the pressure gradient in the direction of flow x, μ, and ρ are the dynamic viscosity and density of the liquid, respectively, k and t are the permeability and thickness of the porous material, respectively, and g is the gravitational acceleration. The first term on the right-hand side represents the pressure drop due to viscous losses, and the second term represents the pressure drop due to gravity.

Equating the capillary pressure with the gravitational and viscous pressure drops requires integration of Eq. (3). The boundary conditions for the resultant pressure distribution are that (i) the pressure at the base of the interior region is equal to the capillary pressure P_c, and (ii) the pressure as a function of height is continuous at the interface between the interior and exterior regions. These boundary conditions can be written as,

$$P(x = 0) = P_c \tag{4}$$

$$P_{int}(x = h_i) = P_{ext}(x = h_i) \tag{5}$$

Substituting Eqs. (1) and (2) into Eq. (3) and applying the boundary conditions (4) and (5) yields the following expressions for the pressure P as a function of location x for the interior (P_{int}) and exterior (P_{ext}) pressures:

$$P(x) = P_c - \frac{2\mu\dot{m}_e''}{tk\rho}x_c x - \rho g x \text{ for } 0 \le x \le h \tag{6}$$

$$P(x) = P_c - \frac{2\mu\dot{m}_e''}{tk\rho}\left(x_c x - \frac{1}{2}(x - h)^2\right) - \rho g x \text{ for } h \le x \le h + x_c \tag{7}$$

The critical wetting length exists such that the capillary, viscous, and gravitational forces are balanced. Thus, setting the left-hand side of Eq. (7) equal to zero and rearranging yields a quadratic equation for the critical wetting length x_c, which can then be written as,

$$x_c = \frac{-b \pm \sqrt{b^2 - 4ac}}{2a} \tag{8}$$

where $a = -\mu \dot{m}_e'' / tk\rho$, $b = -\rho g - 2\dot{m}_e'' \mu h_i / tk\rho$, and $c = P_c - \rho g h_i$. The flow rate through the interior region is then given by Eq. (1).

Moreover, the capillary pressure P_c is given by the Laplace equation (de Gennes et al. 2004):

$$P_c = \frac{2\sigma \cos\theta}{r}, \tag{9}$$

where σ is the surface tension of the liquid and θ is the contact angle between the nutrient medium and the bulk solid membrane material. Furthermore, the hydraulic permeability k was estimated as a function of the average pore radius r and void fraction ϵ, as these properties are conventionally reported by membrane manufacturers. The Millington model was used, and the permeability is given by Millington and Quirk (1961),

$$k = 1/8\epsilon^{4/3} r^2 \tag{10}$$

Finally, for all simulations, the height of the interior region h_i was 10 cm, typical of porous substrate bioreactors reported in the literature (Murphy et al. 2012; Naumann et al. 2013; Liu et al. 2013).

2.2.1 *Evaporative Flux from the Exterior Membrane*

The evaporative flux from the membrane in the exterior region, $\dot{m}_e''$, is a function of the temperature of the membrane, which is in turn dependent on the evaporative flux. Therefore, the following energy balance was utilized to determine the steady-state rib surface temperature T_r as a function of environmental conditions:

$$\alpha G_r + h_c(T_\infty - T_r) - k_\omega \left(\omega_r(T_r) - \omega_\infty(T_\infty)\right) h_{fg} = 0, \tag{11}$$

where α is the total absorptivity of the rib with respect to the incident radiation G_r, h_c, and k_ω are the heat and mass transfer coefficients between the rib surface and the surrounding air, and ω_r and ω_∞ are the mass fractions of water vapor at the rib surface and in the ambient air, respectively, which are functions of the rib surface temperature and ambient air temperature, T_r and T_∞, respectively. Furthermore, h_{fg} is the heat of vaporization of water. The three terms on the left-hand side of Eq. (11) represent the rates of radiative heating, convective heating, and evaporative cooling, respectively. Equation (11) was solved iteratively for the rib surface temperature T_r, and the evaporative flux $\dot{m}_e''$ was calculated as,

$$\dot{m}_e'' = k_\omega \left(\omega_r(T_r) - \omega_\infty(T_\infty)\right), \tag{12}$$

where the mass fraction of water vapor in the ambient air $\omega_\infty(T_\infty)$ was calculated based on the air temperature T_∞ and the relative humidity RH. Moreover, the mass transfer coefficient k_ω was calculated from the Sherwood number as Bird et al. (1960),

$$Sh = \frac{k_\omega x_c}{\rho_a D_{w,a}}, \tag{13}$$

where ρ_a and $D_{w,a}$ are the density of air and the diffusivity of water vapor in air, respectively. In turn, the Sherwood number was calculated taking into account both natural and forced convection using the correlation proposed by Mills (1999):

$$Sh = \left(Sh_n^{7/2} + Sh_f^{7/2}\right)^{2/7} \tag{14}$$

The natural convection Sherwood number, Sh_n, was calculated using the correlation proposed by Incropera et al. (2007),

$$Sh_n = \frac{0.68 + 0.67 Sc^{1/4} Gr^{1/4}}{(1 + (0.492/Sc)^{9/16})^{4/9}} \tag{15}$$

where Sc and Gr are the Schmidt and Grashof numbers, respectively. Moreover, the Sherwood number for forced convection, Sh_f, was calculated taking into account both laminar and turbulent flow using the correlation (Incropera et al. 2007),

$$Sh_f = \left(0.037 Re^{4/5} - 871\right) Sc^{1/3}, \tag{16}$$

where Re is the Reynolds number based on the wind speed and the characteristic length of the system. The characteristic length for forced convection was 10 cm, based on the size of a scaled up artificial tree system. The heat transfer coefficient h_c was calculated using the heat and mass transfer analogy (Incropera et al. 2007). To do this, Eqs. (13–16) were used, substituting the Nusselt number for the Sherwood number and the Prandtl number for the Schmidt number.

2.3 Case Study: Membrane Properties and Environmental Parameters

A case study was performed in which the flow rates through typical membranes were investigated for typical environmental conditions. This section describes the physico-chemical properties of the three membranes, as well as the environmental conditions investigated.

2.3.1 Physico-Chemical Properties of Three Porous Membranes

Three commercially available porous membranes were investigated for use as the rib material. The three media investigated were made from surface-modified hydrophilic polyvinylidene fluoride (PVDF), glass fiber, and cellulose. Table 1 summarizes the material properties of these three membranes. The table indicates that the PVDF mem-

Table 1 Material properties, permeability, and maximum available capillary pressure for the three rib materials investigated

	PVDF	Glass fiber	Cellulose
Brand	Millipore	Whatman	Fisher
Product code	DVP00010	GF/AH	P8
Thickness, t (mm)	0.13	0.33	0.20
Pore radius, r (μm)	0.6	1.5	20
Void fraction, ϵ	0.70	0.85	0.87
Contact angle, θ (°)	55[a]	20[b]	39[c]
Permeability, k ($m^2 \times 10^{12}$)	0.028	0.23	42
Capillary pressure, P_c (kPa)	128	91	5.7

[a] Pasquini et al. (2006)
[b] Adham et al. (2006)
[c] Sumner et al. (2004)

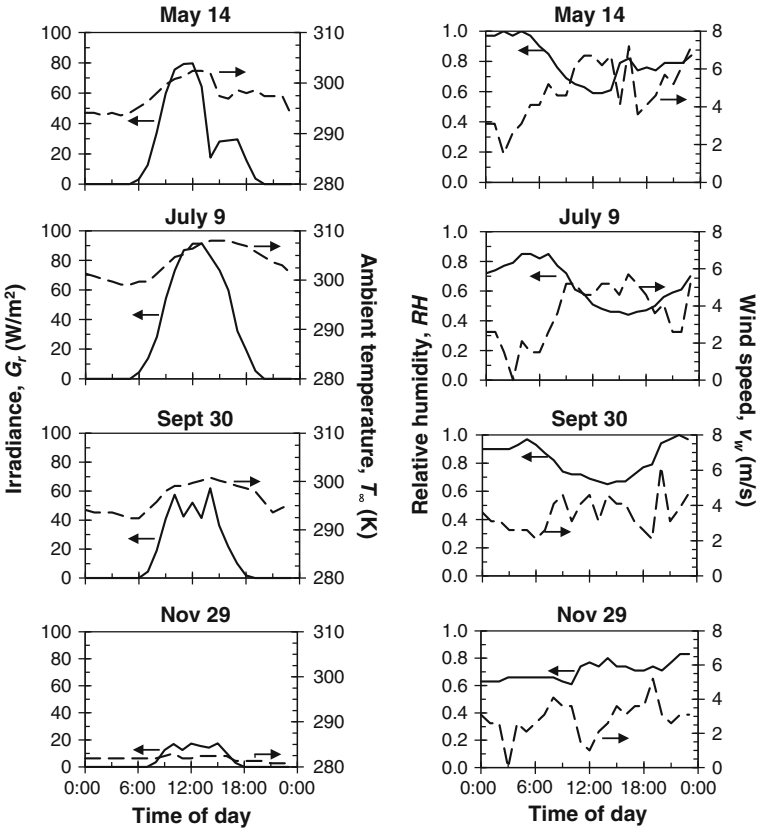

Fig. 2 Irradiance per rib, air temperature, relative humidity, and wind speed for 24-h periods in spring (May 14), summer (July 9), fall (September 30), and winter (November 29) for Memphis, TN, USA (Wilcox and Marion 2008)

brane exerts the greatest capillary pressure, but also has the lowest permeability of the three membranes as a result of it having the smallest pore size. On the other hand, the cellulose paper has the greatest permeability, but the least maximum capillary pressure.

2.3.2 Weather Parameters for Typical Operating Conditions

Four 24-h simulations using weather parameters from representative days of spring, summer, fall, and winter were performed for Memphis, TN, USA. Memphis was selected as the location because its moderately high annual insolation, proximity to water sources, and moderate temperatures make it a good location for algae cultivation. The spring, summer, fall, and winter days were May 14, July 9, September 30, and November 29, respectively. The values for hourly air temperature, irradiance, relative humidity, and wind speed were obtained from the National Renewable Energy Laboratory's Typical Meteorological Year 3 Data, which reports real weather data that is deemed typical of the time span 1991–2005 (Wilcox and Marion 2008). The weather parameters used are shown in Fig. 2. It was assumed that the irradiance onto the rib was equal to 10 % of the

Table 2 Environmental parameters used in the parameter sweep

	Very low	Low	Base	High	Very high
Air temperature, T_∞ (K)	285	290	295	300	305
Relative humidity, RH (%)	0	20	40	60	80
Wind speed, v_w (m/s)	0	2	4	6	8
Irradiance, G_r (W/m^2)	0	20	40	60	80

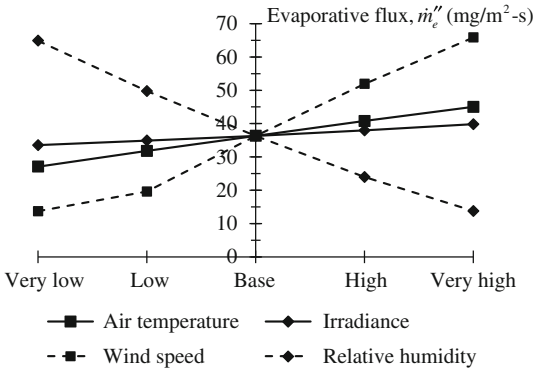

Fig. 3 Effect of varying the irradiance, air temperature, relative humidity, and wind speed on the evaporative flux from the rib

global horizontal irradiance, which takes into account the projected area of the incident sunlight onto the vertical rib. Finally, the total absorptance of each membrane with respect to the solar spectrum was 0.3 based on measurements performed in our laboratory.

3 Results and Discussion

3.1 Effect of Porous Medium Properties and Environmental Parameters on Flow Rate

3.1.1 Range of Expected Evaporative Fluxes

It was first of interest to calculate the range of evaporative fluxes expected for typical outdoor operating conditions. Therefore, a parameter sweep was performed in which the evaporative flux was calculated as the irradiance onto the rib G_r, the ambient temperature T_∞, the relative humidity RH, and the air speed parallel to the rib v_w were individually varied relative to a base case value. Table 2 shows the parameter values investigated in the sweep. Figure 3 shows the effect of varying each parameter on the evaporative flux from the rib, $\dot{m}_e''$. The figure indicates that the evaporative flux in the base case scenario was 36 mg/m^2 s. Moreover, the evaporative flux decreased from 65 to 14 mg/m^2 s as the relative humidity increased from 0 to 80 %. Increasing the wind speed from 0 to 8 m/s caused the evaporative flux to increase from 14 to 66 mg/m^2-s as a result of forced convection. Increasing the air temperature from 285 to 305 K caused the flux to increase from 27 to 45 mg/m^2 s as a result of the increase in water vapor pressure at the rib surface. Finally, increasing the irradiance from 0 to 80 W/m^2 increased the flux from 34 to 40 mg/m^2 s. The results of this analysis provide a range of evaporative fluxes that are necessary for calculating the total flow rate through the rib.

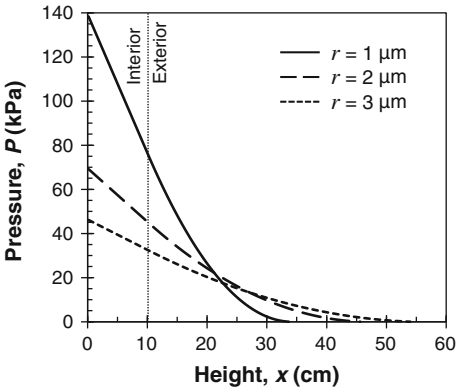

Fig. 4 Pressure distributions within ribs with pore radii of 1, 2, and 3 μm. The contact angle, rib thickness, void fraction, and evaporative flux were 20°, 0.5 mm, 0.8, and 36 mg/m^2 s, respectively

3.1.2 Effects of Porous Medium Properties on Critical Wetting Length and Total Flow Rate

The critical wetting length and total flow rate are critical parameters from an artificial tree design perspective. The total flow rate is an important design parameter as it determines the characteristic length of nutrient exhaustion in the direction of flow (Murphy and Berberoglu 2014). Moreover, the critical wetting length is important as it determines the necessary geometric dimensions of the rib. Thus, this section focuses on the dependence of these two parameters on physico-chemical properties of the porous membrane.

It is first of interest to investigate the pressure distribution in the rib, as this distribution dictates the critical wetting length and total flow rate. Figure 4 shows the pressure distributions in three hypothetical ribs with pore radii of 1, 2, and 3 μm. The contact angle θ, rib thickness t, and porous membrane void fraction ϵ were constant at 20^o, 0.5 mm, and 0.8, respectively. The evaporative flux was 36 mg/m^2 s, which was the base case flux from the evaporative flux model. The figure indicates that decreasing the pore radius increased the maximum capillary pressure that the membrane could provide, as the maximum pressures in the membranes with pore radii of 1, 2, and 3 μm were 138, 69, and 46 Pa, respectively. However, decreasing the pore radius also caused greater viscous losses to occur, as the pressure gradients in the interior region of the three membranes were −6.3, −2.4, and − 1.4 kPa/cm, respectively. Therefore, for vertically oriented PSBRs, a pore radius must be sought that is small enough to provide ample capillary pressure but large enough to diminish viscous losses.

A pore radius was sought that would maximize the flow through the rib. For this, the critical wetting length and flow rate were calculated for hypothetical ribs with different pore radii r and contact angle θ. The pore radius varied between 100 nm and 1 mm and the contact angle varied between 0°, which represents the material capable of providing the maximum possible capillary pressure, and 85^o. The void fraction and membrane thickness were held constant at 0.8 and 0.5 mm, respectively. Finally, evaporative fluxes investigated were 14 and 66 mg/m^2 s, which represented the minimum and maximum fluxes observed in the evaporative flux analysis.

Figure 5 shows the effect of pore radius and wetting angle on the critical wetting length and flow rate. The wetting length and flow rate were each inversely related to the contact angle, which was expected as perfectly wetting materials (contact angle of zero) provide the maximum possible capillary pressure. Moreover, the wetting length and flow rate each approached zero as the contact angle approached 90°, indicating that only hydrophilic materials can be used as substrates for artificial trees. Moreover, as the evaporative flux increased,

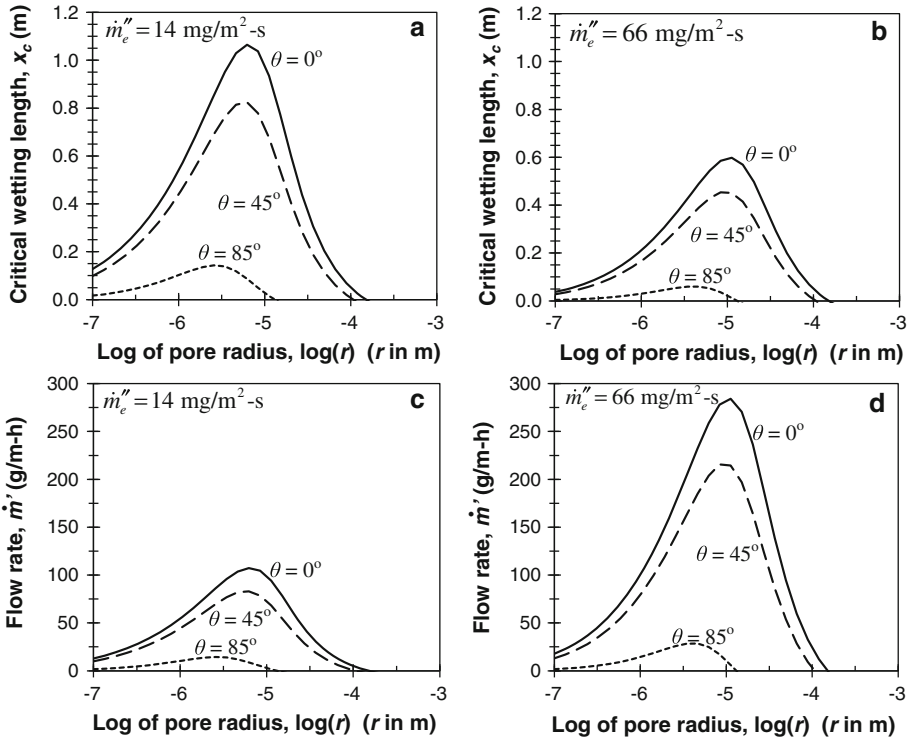

Fig. 5 Effect of pore radius and contact angle on critical wetting length and flow rate

the critical wetting length decreased, while the flow rate through the rib increased. The maximum critical wetting lengths for the slow (14 mg/m^2 s) and fast (66 mg/m^2 s) evaporation cases were 1.1 and 0.60 m, and these wetting lengths corresponded to flow rates of 110 and 280 g/m h, respectively.

Figure 5 also indicates that there was a pore radius that maximized the flow rate through the rib. This occurred because the capillary pressure is inversely related to pore radius, whereas the permeability is proportional to the square of the pore radius. For the slow evaporation case, the optimal pore radii for materials with contact angles of 0°, 45°, and 85° were 7, 6, and 3 μm, respectively. Increasing the contact angle decreased the capillary pressure, thereby reducing the wetting length, and therefore, the total flow rate, reducing viscous losses and allowing for smaller pore diameters. For the fast evaporation case, the optimal pore diameters for the contact angles of 0°, 45°, and 85° were 11, 9, and 5 μm, respectively. Therefore, porous membranes with pore radii of about 10 μm should be used for maximizing flow through artificial trees.

3.2 Case Study Results: Daily and Annual Variations in Critical Wetting Length and Total Flow Rate

Figure 6 shows the critical wetting length and total flow rate for the PVDF membrane for spring, summer, fall, and winter simulations. As the evaporative flux decreased, the critical wetting length increased, while the total flow rate decreased. On May 14, this effect was highly pronounced at 2:00 AM and 4:00 AM, as the evaporative flux approached zero and

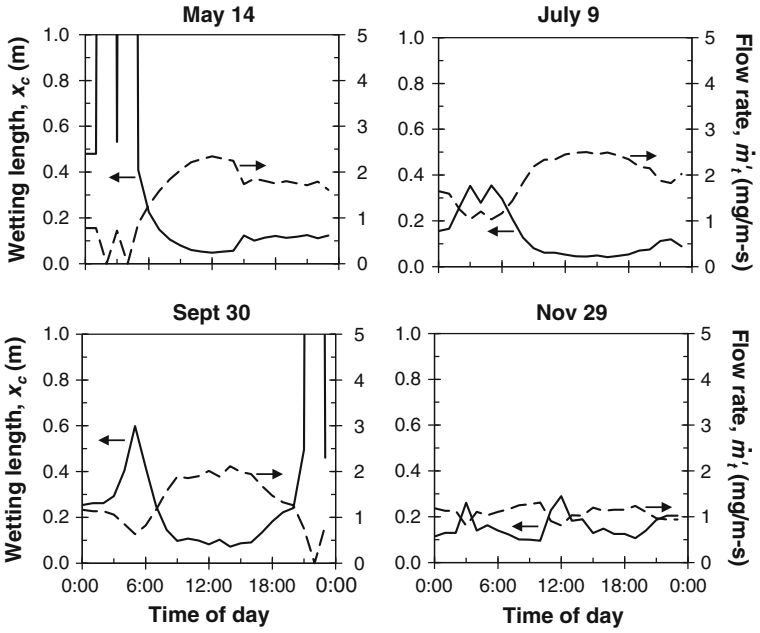

Fig. 6 Critical wetting length and total flow rate through the PVDF rib throughout the 24-h simulations for the spring, summer, fall, and winter

the critical wetting length approached 13 m, which is the height at which the capillary pressure balances the hydrostatic pressure in the absence of viscous losses. For the 24-h simulations of spring, summer, fall, and winter, the daily evaporative flow rates were 0.14, 0.16, 0.12, and 0.10 l per meter of rib length per day, respectively.

Moreover, Fig. 7 indicates that the daily variation in the critical wetting length and flow rate for the glass fiber rib were qualitatively similar to those for the PVDF rib, although their magnitudes were about 4.5 times greater for the glass fiber rib. Therefore, although the PVDF membrane can exert a capillary pressure 1.4 times greater than the glass fiber membrane, the effect of increased capillary pressure on flow rate is negated by the hydraulic permeability for the glass fiber membrane being about eight times greater than that of the PVDF membrane.

Furthermore, Fig. 8 indicates that the critical wetting length for the cellulose rib for all 24-h simulations remained within 27 % of its maximum value of 47 cm, which corresponds to the balance of capillary and hydrostatic pressures. As a result of the relatively constant critical wetting length, the total flow rate was more sensitive to environmental changes than for the other two membranes. For example, for July 9, the total flow rate deviated from the average by as much as 106 % for the cellulose membrane, whereas the deviation from the average was only 46 and 69 % for the PVDF and glass fiber membranes, respectively. Averaged over the four 24-h simulations, the flow rates through the ribs made of PVDF, glass fiber, and cellulose were 1.5, 7.4, and 6.3 mg/m s, respectively.

The cellulose rib represents a regime shift from the PVDF and glass fiber ribs in that the flow rate through the cellulose rib was gravity limited rather than viscosity limited. The PVDF and glass fiber ribs were able to provide high capillary pressures of 128 and 91 kPa, respectively. As a result, when the evaporative flux decreased as a result of changing environmental conditions, the capillary pressure was able to overcome gravity, thereby increasing the

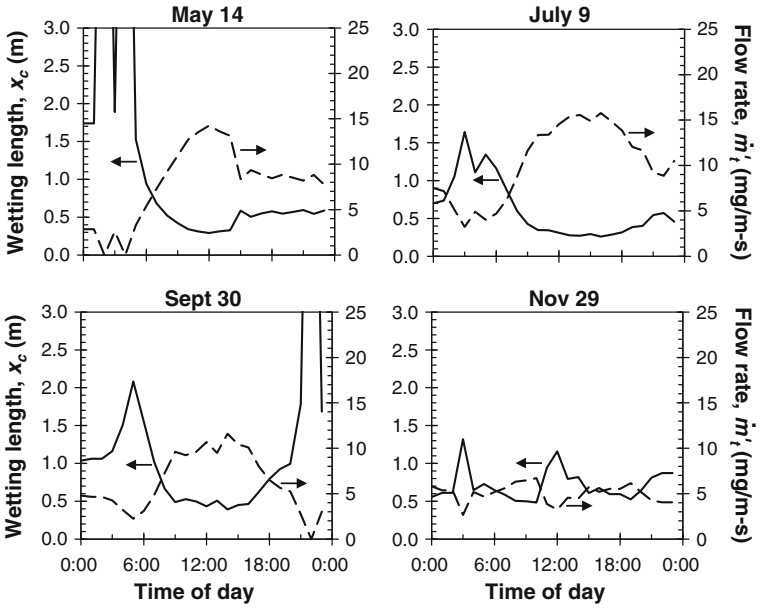

Fig. 7 Critical wetting length and total flow rate through the glass fiber rib throughout the 24-h simulations for the spring, summer, fall, and winter

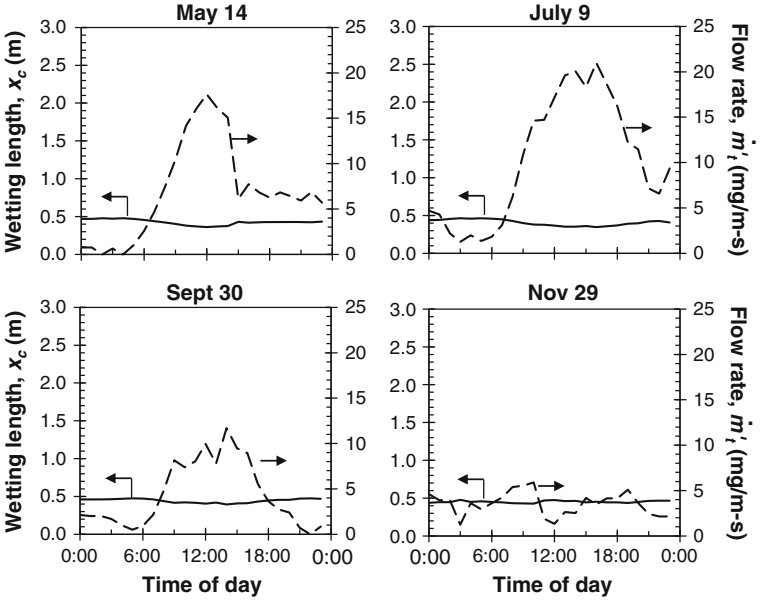

Fig. 8 Critical wetting length and total flow rate through the cellulose rib throughout the 24-h simulations for the spring, summer, fall, and winter

critical wetting length and making the total flow rate relatively insensitive to the evaporative flux. On the other hand, the capillary pressure exerted by the cellulose membrane was only 5.7 kPa. As a result, when the evaporative flux decreased, the critical wetting length was

not able to increase to maintain a relatively constant flow rate. Therefore, evaporation from gravity limited membranes, such as this cellulose membrane, is similar to pool evaporation, in which the evaporative surface area is constant, whereas viscosity limited membranes, such as the PVDF and glass fiber membranes, adjust their evaporative surface area in response to changing evaporative flux to maintain a more consistent total flow rate.

3.3 Implications for Algae Cultivation

In this section, the results for flow rate as a function of membrane properties and environmental conditions are placed in the context of algae cultivation. Artificial tree-cultivating algae consist of interior rib regions that host microbial growth and exterior regions that serve as evaporative pumps. Therefore, when designing these systems, it is of interest to provide a nutrient medium flow rate that sustains sufficient nutrient delivery rates to the biofilm, while controlling evaporative water losses.

As nutrient medium flows through the porous membrane from the reservoir toward the evaporation region, nutrient concentrations in the bulk liquid decrease as nutrients diffuse into the biofilm and get consumed by the cells. The nutrient delivery length was previously defined as the length in the direction of flow at which the lack of availability of one or more nutrients inhibits the growth rate by 50 % compared to the growth rate in a nutrient-replete environment (Murphy and Berberoglu 2014). From a design perspective, the scales of the nutrient delivery length and the physical height of the interior region cultivating cells should be equal. If the nutrient delivery length is significantly shorter than the rib height, dead zones will occur downstream, whereas if the nutrient delivery length is significantly longer than the rib height, excessive water will be lost by evaporation.

It was previously shown that the nutrient delivery length, x_{ND}, could be expressed as (Murphy and Berberoglu 2014),

$$x_{\mathrm{ND}} = C\frac{\left(\dot{m}'/\rho\right)[i_{\mathrm{L}}]_o}{\dot{X}_o''/Y_{X/i_{\mathrm{L}}}}, \tag{17}$$

where C is a constant of proportionality based on growth kinetics, $\dot{m}'$ is the mass flow rate per unit depth, ρ is the density of nutrient medium, $[i_L]_o$ is the concentration of the limiting nutrient in fresh nutrient medium, $\dot{X}_o''$ is the areal biomass production rate under nutrient replete conditions, and $Y_{X/i_{\mathrm{L}}}$ is the biomass yield based on consumption of the growth limiting nutrient. Equation (17) indicates that the limiting nutrient influx to the reactor balances the rate of its consumption.

As an example, consider the design of an artificial tree for cultivating the cyanobacteria *Anabaena variabilis* in the BG11 nutrient medium. First, the limiting nutrient was identified as phosphate, which had a concentration $P_{T,o}$ of 0.23 mM in fresh BG11 Andersen (2005) and a biomass yield, $Y_{X/P}$, of 4280 grams dry weight per mole of phosphate consumed for *A. variabilis* (Murphy and Berberoglu 2014). From previous experimental data, it was found that the biomass production rate undser nutrient-replete conditions, $\dot{X}_o''$, of a 40 μm thick *A. variabilis* biofilm under an irradiance of 24 W/m^2 was 0.1 g/m^2 h, and that the coefficient C was equal to 0.2 based on microbial kinetics (Murphy and Berberoglu 2014). Rearranging Eq. (17) for the mass flow rate and then setting the nutrient delivery length equal to the height of the biofilm cultivating region h_i, which was 0.1 m in this analysis, yields the relationship:

$$\dot{m}' = \frac{h_i \dot{X}_o'' \rho}{C Y_{X/i_{\mathrm{L}}}[i_{\mathrm{L}}]_o} \tag{18}$$

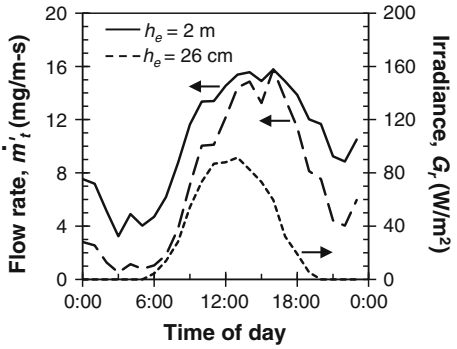

Fig. 9 Flow rates through glass fiber ribs with exterior heights of 26 cm and 2 m, as well as the irradiance, throughout the day of July 9

Using the above parameter values in Eq. (18) yields a mass flow rate requirement of 50 g/m^2 h for the nutrient medium to prevent nutrient limitation to cells. Furthermore, the selection of the porous medium suitable for this mass flow rate also depends on the evaporative flux of water from the exterior region. For example, for a slow evaporative flux of 14 mg/m^2 s, a porous membrane with an external region length of 0.5 m with a thickness, contact angle, void fraction, and pore radius of 0.5 mm, 45°, 0.8, and 1.6 μm, respectively, would be needed (Fig. 5a, c). Note that at this evaporative flux case, the exterior length required is five times longer than the interior region, which can raise concerns over material costs and biofilm shading. On the other hand, at a faster evaporative flux of 66 mg/m^2 s, a porous membrane of exterior length 0.1 m with a thickness, contact angle, void fraction, and pore radius of 0.5 mm, 45°, 0.8, and 0.3 μm, respectively would be required (Fig. 5b, d).

A fortuitous aspect of artificial trees is that the flow rate through the reactor closely follows the daily variation in irradiance, which drives growth. Because the nutrient delivery length is directly related to the flow rate and inversely related to the growth rate, the correlation between flow rate and irradiance serves to maintain the nutrient delivery length consistent throughout the day. In other words, artificial trees provide a passive mechanism for tuning the rate of nutrient delivery to the rate of photon-driven nutrient consumption.

Moreover, designing the length of the exterior region to be equal to the minimum expected critical wetting length enables water conservation without sacrificing productivity. This occurs because the critical wetting length is inversely related to the flow rate, and the temporal variation in flow rate closely follows the temporal variation in irradiance. Therefore, truncating the exterior region to its minimum wetting length enables fast nutrient delivery during the day when photons are available, while mitigating evaporative losses at night.

To demonstrate the effectiveness of this strategy, Fig. 9 shows the irradiance onto, as well as the flow rate through, the glass fiber rib on July 9. Two cases for flow rate are shown. The tall rib had an exterior length of 2 m, which was greater than the maximum daily critical wetting length. The short rib had an exterior length of 26 cm, which was equal to the minimum daily critical wetting length. The figure indicates that the flow rate through the short rib was as much as 84 % less than the flow rate through the long rib at night when the irradiance was zero. However, between the hours of 10:00 AM to 4:00 PM, the flow rate through the short rib was within 25 % of the flow rate through the long rib. The daily evaporative water losses for the long and short ribs were 0.89 and 0.61 L/m day, respectively. Thus, setting the exterior membrane height equal to the minimum expected wetting length can decrease daily evaporative losses by about 31 % without significantly sacrificing productivity.

Additionally, one criterion that made Memphis a candidate for siting the artificial tree was its high annual humidity, which reduces the evaporative losses compared to less humid

climates, which can be desirable for operation of conventional open bioreactors. However, because the productivity of artificial trees scales with the evaporation rate, they are probably better suited for less humid climates, which would increase the flow rate through the ribs, while decreasing the critical wetting length. However, less humid climates tend to have fewer water resources than more humid ones, so the relative scarcity of water between different sites should carefully be taken into account.

4 Conclusions

The flow rate through an artificial tree, also known as an evaporation-driven Porous Substrate Bioreactor (PSBR), was modeled. Artificial trees cultivate algal cells as biofilms on porous, wicking membranes, the flow through which is driven by evaporation. These reactors are advantageous over conventional reactors in that they passively deliver water and nutrients to the microorganisms without requiring a pump. First, a coupled heat and mass transfer analysis was performed to calculate the evaporative flux from the membrane surface for a range of environmental conditions. Using this range of evaporative fluxes, it was determined that the porous membrane pore radius that maximized flow through the artificial tree was about 10 μm. This optimal size resulted from the competition between increased capillary pressure and decreased permeability with decreasing pore radius. Then, a case study was performed in which the flow rates through three commercially available porous membranes were calculated. Four 24-h simulations were performed for the spring, summer, fall, and winter in Memphis, TN. Averaged over the four 24-h simulations, the flow rates through the ribs made of PVDF, glass fiber, and cellulose were 0.13, 0.64, and 0.54 l per meter per day, respectively. The glass fiber rib had the greatest flow rate because it was able to provide high capillary pressure (92 kPa), while having relatively high permeability (0.23×10^{-12} m^2). On the other hand, the PVDF and cellulose materials suffered from low permeability and low capillary pressure, respectively. It was observed that in outdoor systems, the flow rate and biofilm growth rate are both directly related to the irradiance, which provides a passive mechanism for efficient nutrient delivery. A design strategy was then outlined for matching the length scale of the biofilm with the length scale of nutrient delivery as dictated by the nutrient medium flow rate. This strategy enables design of highly productive artificial trees without excessive evaporative water loss.

Acknowledgments The authors would like to sincerely thank Dr. Carlos Hidrovo for his helpful discussions. The authors also gratefully acknowledge the financial support of the National Science Foundation (CBET-1125755) making this study possible.

References

Adham, S., Chiu, K.-P., Lehman, G., Mysore, C., Clouet, J.: Optimization of Membrane Treatment for Direct and Clarified Water Filtration, 1st edn. American Waterworks Foundation, New York (2006)

Andersen, R.A.: Algal Culturing Techniques. Elsevier Academic Press, London (2005)

Beal, C.M., Smith, C.H., Webber, M.E., Ruoff, R.S., Hebner, R.E.: A framework to report the production of renewable diesel from algae. Bioenergy Res. **4**, 36–60 (2011)

Bird, R.B., Stewart, W.E., Lightfoot, E.N.: Transport Phenomena, 1st edn. Wiley, New York (1960)

Borowitzka, M.A.: Commercial production of microalgae: ponds, tanks, tubes, and fermenters. J. Biotechnol. **70**, 313–321 (1999)

Chisti, Y.: Biodiesel from algae. Biotechnol. Adv. **25**, 294–306 (2007)

Chisti, Y., Yan, J.: Energy from algae: current status and future trends. Appl. Energy **88**(10), 3277–3279 (2011)
Clarens, A.F., Resurreccion, E.P., White, M.A., Colosi, L.M.: Environmental life cycle comparison of algae to other bioenergy feedstocks. Environ. Sci. Technol. **44**(5), 1813–1819 (2010)
Craggs, R.J., Heubeck, S., Lundquist, T.J., Benemann, J.R.: Algal biofuels from wastewater treatment high rate algal ponds. Water Sci. Technol. **63**(4), 660–665 (2011)
Day, J.G., Benson, E.E., Fleck, R.A.: In vitro culture and conservation of microalgae: applications for aquaculture, biotechnology and environmental research. In Vitro Cell Dev. Biol. **35**, 127–136 (1999)
de Gennes, P.-G., Brochard-Wyart, F., Quere, D.: Capillarity and Wetting Phenomena: Drops, Bubbles, Pearls, Waves, 1st edn. Springer, New York (2004)
Incropera, F.P., Dewitt, D.P., Bergman, T.L., Lavine, A.S.: Fundamentals of Heat and Mass Transfer, 6th edn. Wiley, Hoboken (2007)
Jorquera, O., Kiperstok, A., Sales, E.A., Embiruçu, M., Ghirardi, M.L.: Comparative energy life-cycle analyses of microalgal biomass production in open ponds and photobioreactors. Bioresour. Technol. **101**(4), 1406–1413 (2010)
Kaviany, M.: Principles of Heat Transfer in Porous Media, 2nd edn. Springer, New York (1999)
Kumar, K., Dasgupta, C.N., Nayak, B., Lindblad, P., Das, D.: Development of suitable photobioreactors for CO_2 sequestration addressing global warming using green algae and cyanobacteria. Bioresour. Technol. **102**(8), 4945–4953 (2011)
Liu, T., Wang, J., Hu, Q., Cheng, P., Ji, B., Liu, J., Chen, Y., Zhang, W., Chen, X., Chen, L., Gao, L., Ji, C., Wang, H.: Attached cultivation technology of microalgae for efficient biomass feedstock production. Bioresour. Technol. **127**, 216–222 (2013)
Milledge, J.J.: Commercial application of microalgae other than as biofuels: a brief review. Rev. Environ. Sci. Biotechnol. **10**(1), 31–41 (2010)
Millington, R.J., Quirk, J.P.: Permeability of porous solids. Trans. Faraday Soc. **57**, 1200–1207 (1961)
Mills, A.F.: Heat Transfer, 5th edn. Prentice-Hall, Upper Saddle River (1999)
Murphy, T.E., Berberoglu, H.: Flux balancing of light and nutrients in a biofilm pho- tobioreactor for maximizing photosynthetic productivity (accepted manuscript). Biotech- nol. Prog (2014)
Murphy, T.E., Fleming, E., Bebout, L., Bebout, B., Berberoglu, H.: A novel micro- bial cultivation platform for space applications. In: 1st Annual International Space Station Research and Development Conference, Denver (2012)
Naumann, T., Cebi, Z., Podola, B., Melkonian, M.: Growing microalgae as aquaculture feeds on twin-layers, a novel solid state photobioreactor. J. Appl. Phycol. **25**, 1619 (2013)
Ozkan, A., Kinney, K., Katz, L., Berberoglu, H.: Reduction of water and energy requirement of algae cultivation using an algae biofilm photobioreactor. Bioresour. Technol. **114**, 542–548 (2012)
Pasquini, D., Belgacem, M.N., Gandini, A., da Silva Curvelo, A.A.: Surface esterification of cellulose fibers: characterization by DRIFT and contact angle measurements. J. Colloid Interface Sci. **295**(1), 79–83 (2006)
Pulz, O., Gross, W.: Valuable products from biotechnology of microalgae. Appl. Microbiol. Biotechnol. **65**(6), 635–648 (2004)
Scott, S.A., Davey, M.P., Dennis, J.S., Horst, I., Howe, C.J., Lea-Smith, D.J., Smith, A.G.: Biodiesel from algae: challenges and prospects. Curr. Opin. Biotechnol. **21**(3), 277–286 (2010)
Spolaore, P., Joannis-Cassan, C., Duran, E., Isambert, A.: Commercial applications of microalgae. J. Biosci. Bioeng. **101**(2), 87–96 (2006)
Sumner, A.L., Menke, E.J., Dubowski, Y., Newberg, J.T., Penner, R.M., Hemminger, J.C., Wingen, L.M., Finlayson-Pitts, B.J.: The nature of water on surfaces of laboratory systems and implications for heterogeneous chemistry in the troposphere. Phys. Chem. Chem. Phys. **6**, 604–613 (2004)
Wilcox, S., Marion, W.: Users manual for TMY3 data sets. Technical report, National Renewable Energy Laboratory, Golden (2008)